On the Estimation of Angle Rate in Radar

Jeffrey A. Nanzer, *Senior Member, IEEE,* and Matthew D. Sharp, *Member, IEEE*

***Abstract*— The direct measurement of the angle rate of moving objects using a radar with a spatially diverse electric field pattern, a measurement analogous to the measurement of the range rate of a moving objects, represents, along with the measurements of range, range rate, and angle, a fourth basic radar measurement. Recently introduced and experimentally demonstrated, the theoretical accuracy of the direct measurement of angle rate is derived in this paper, and it is compared to the measurements of range, range rate, and angle in the context of the optimal signal forms for the best measurement accuracy. Signal forms achieving optimal accuracy for each measurement are discussed; example implementations of high-accuracy measurements are compared to the optimal forms; and the limitations of simultaneous measurements of pairs of measurements are derived. Combining the angle rate measurement with the three other standard radar measurements may provide future radar systems the capability to simultaneously and instantaneously measure the position and 3-D trajectory of moving objects without compromising the accuracy of any individual measurement.**

***Index Terms*— Accuracy, angle rate, interferometry, radar, radar measurements.**

I. Introduction

THE accurate measurement of the location of an object is of critical importance in remote sensing, as is accurate measurement of the trajectory of the object. Often times in remote sensing of moving objects, the current position is not as critical a piece of information as is the estimated position at some time in the future. Whereas the measurement of the object's range and angle gives the current position relative to the measuring sensor, the measurement of the time rate of change of the object's range and angle yields an estimate of the trajectory of the object. Such trajectory measurements are fundamental inputs to target tracking algorithms, such as Kalman filters, which are used to estimate the future position of a moving object. It is thus important that the sensor yield a measurement of the object's trajectory, in all dimensions (range rate and two dimensions of angle rate) if possible, with the best achievable accuracy.

Electromagnetic remote sensors, radars in particular, although passive radiometers are also used, provide a means for achieving long-range measurements of an object's position and trajectory. Radar systems generally measure range, range rate, and angle, and although angle rate can then be calculated from repeated measurements of the angle, there is traditionally no direct angle rate measurement possible. Recently, however, the authors introduced [1] and demonstrated [2] a radar system that directly measures the angle rate of moving objects in addition to simultaneously measuring the range rate, thereby introducing the possibility of measuring the 3-D trajectory of moving objects directly. The measurement method in [2] utilized a spatially diverse receiving aperture to directly measure the angle rate of moving objects without tracking. While the angle of the object is not directly measured, the measurement of the angle rate is mathematically identical to the measurement of the range rate (that is, the Doppler frequency of the return signal), and thus can be performed directly without significant signal processing. Coherent spatially diverse radar apertures are traditionally atypical; however, recent significant advances in digital array technologies now make it feasible to implement the simple angle rate measurement in a single radar receiving aperture. But because the resolution of the measurement of angle and angle rate is dependent on the spatial frequency sampled by the aperture [3], and is therefore improved with a longer antenna dimension, widely separated antennas can provide better resolution of angle rate than a single aperture. The current drive toward coherent distributed RF systems [4]–[8] provides a direct means for implementing long-baseline angle rate measurements to yield extremely high-resolution angle and angle rate measurements. While longer antenna baselines provide for improved angle rate *resolution* for a system such as that described in [1]–[3], the *accuracy* with which angle rate can be measured and the optimal form for measuring the accuracy has not been investigated.

This paper derives the theoretical bound on accuracy in angle rate measurements in electromagnetic receivers, within the context of the theoretical bounds on the traditional radar measurements of range, range rate, and angle. The primary contributions are a derivation of the optimal signal form for the recently introduced angle rate measurement method, and a new analysis showing that the optimal signal form for measurement accuracy is mathematically identical across all four radar measurements, differing only in the domain of implementation. Whereas radar is the primary application, the presented results apply equally to passive radiometers and receivers in general. System-level implications of the optimal apertures for the four radar measurements are discussed and compared to examples of systems in the literature.

This paper is organized as follows. In Section II, the theoretical bounds on accuracy for the measurements of range, range rate, angle, and angle rate are derived, from the point of view of a continuous time waveform and continuous aperture; typically these bounds are analyzed in the discrete-time

Manuscript received October 12, 2015; revised August 9, 2016; accepted December 9, 2016. Date of publication December 28, 2016; date of current version March 1, 2017.

J. A. Nanzer is with the Department of Electrical and Computer Engineering, Michigan State University, East Lansing, MI 48824 USA (e-mail: nanzer@ieee.org).

M. D. Sharp is with the Johns Hopkins University Applied Physics Laboratory, Laurel, MD 20723 USA.

Color versions of one or more of the figures in this paper are available online at http://ieeexplore.ieee.org.

Digital Object Identifier 10.1109/TAP.2016.2645785

and discrete-aperture (array) format, but as will be shown, important insight into the optimal design of the waveforms and apertures for the best accuracy measurements is gained from considering the continuous forms of these bounds, and is otherwise lost in the discrete forms. Section III examines the optimal form of the Fourier domain representation of the signal distributions, and Section IV discusses implementations of the four measurements. In Section V, the relationship of the parameters affecting the simultaneous measurement of range and range rate or angle and angle rate are discussed.

II. Accuracy of Radar Measurements

Radar measurements may be expressed in the general form

$$s_r(x) = s(x;\boldsymbol{u})\alpha + w(x) \tag{1}$$

where $s(x;\boldsymbol{u})$ is a function of the unobservable parameters $\boldsymbol{u} = [u_1, \ldots, u_P]$ that are to be estimated. The complex deterministic parameter α incorporates amplitude and phase fluctuations due to scattering, path loss, beam pattern, etc. The noise $w(x)$ is complex bandpass white Gaussian noise with $\mathbb{E}\{w(x)w^*(u)\} = N_o\delta(x-u)$. It is assumed that the observation period of $s_r(x)$ is sufficient to cover the majority of the support of $s(x;\boldsymbol{u})$ (that is, the majority of the nonzero signal contributions are observed). The following examines the case of $P = 2$ unknown parameters in the vector $\boldsymbol{u}$.

The theoretical accuracy of a radar measurement is given by the variance of the estimate of the parameter of interest for the measurement, such as time or frequency, which can be lower bounded by the Cramer–Rao bound (CRB). Although the CRB may not always be achievable (especially for certain estimators), the form of the CRB can provide insight into the optimal design of the signal to be used such that the variance is reduced, and the measurement accuracy is improved. Of interest is the analysis of the CRB for the unknown parameters $\boldsymbol{u}$, assuming an unknown but deterministic parameter α. For the case where $\boldsymbol{u} = [u_1, u_2]$ the following expression can be derived [9]:

$$\begin{aligned}&\mathrm{var}(\hat{u}_p - u_p)\\ &\geq \frac{N_o}{2|\alpha|^2}\left(\int\left|\frac{\partial s(x;\boldsymbol{u})}{\partial u_p}\right|^2 dx - \frac{1}{E_s}\left|\int \frac{\partial s(x;\boldsymbol{u})}{\partial u_p}^* s(x;\boldsymbol{u})dx\right|^2\right)^{-1}\end{aligned} \tag{2}$$

where $E_s \triangleq \int |s(x;\boldsymbol{u})|^2 dx$.

In the following sections, the above bound is examined for various problems commonly encountered in radar. Beginning with the common range and radial velocity estimation problems, the analogous formulations for angle estimation and angular velocity estimation are then shown.

A. Range and Radial Velocity Measurement

One of the primary measurements made by a radar system is the measurement of range to some object, accomplished by measuring the time delay between the transmission and reception of a signal after reflecting off the object of interest. With the two-way flight time τ the range can be calculated through $R = c\tau/2$. Letting $u_1 = \tau$ (the error in range is easily computed once the error in time delay is computed) yields

$$s_r(t) = g(t-\tau) + w(t) \tag{3}$$

where $g(t)$ is the transmitted signal.

For most narrowband signals, radially moving targets can be modeled as a frequency shift on the scattered signal. For an object radially inbound toward the radar with velocity $v \ll c$, the received signal is modeled as

$$s_r(t) = \alpha g(t-\tau)e^{j2\pi f_d t} + w(t) \tag{4}$$

where $f_d = 2((f_c v)/c)$ and f_c is the RF center frequency of the signal, and the term α is a constant that incorporates the phase shift of the carrier due to the initial range, i.e., $e^{j2\pi f_c \tau}$. In many cases, the range may have already been determined with enough accuracy to ensure that the observations include the majority of the support of $g(t-\tau)$.

In the context of time delay estimation, (2) is evaluated using the model (4) where $s(x;\boldsymbol{u}) = g(t-\tau)e^{j2\pi f_d t}$ and $\boldsymbol{u} = [\tau, f_d]$. The first integral in (2) is

$$\begin{aligned}\int\left|\frac{\partial s(x;\boldsymbol{u})}{\partial u_1}\right|^2 dx &= \int\left|\frac{\partial}{\partial\tau}g(t-\tau)\right|^2 dt\\ &= \int\left|\frac{\partial}{\partial\tau}G(f)e^{-j2\pi f\tau}\right|^2 df\\ &= \int (2\pi f)^2|G(f)|^2 df\\ &\triangleq \zeta_f^2.\end{aligned} \tag{5}$$

The term ζ_f^2 is often called the mean-square bandwidth, and is the second moment of the energy spectrum. Likewise, the second integral is easily evaluated using Plancherel's theorem as

$$\begin{aligned}&\left|\int\left(\frac{\partial s(x;\boldsymbol{u})}{\partial u_1}\right)^* s(x;\boldsymbol{u})dx\right|^2\\ &= \left|\int\left(\frac{\partial}{\partial\tau}g(t-\tau)\right)^* g(t-\tau)dt\right|^2\\ &= \left(\int 2\pi f|G(f)|^2 df\right)^2\\ &= \mu_f^2.\end{aligned} \tag{6}$$

The term μ_f^2 is often referred to as the first moment of the energy spectrum or the mean frequency. From (2), the error in estimating the time-delay is

$$\mathrm{var}(\hat{\tau}-\tau)\} \geq \frac{N_o}{2|\alpha|^2\left(\zeta_f^2 - \frac{1}{E_s}\mu_f^2\right)}. \tag{7}$$

For signals which display the symmetry $|G(f)| = |G(-f)|$, the mean frequency μ_f is zero and the second term in the denominator can be ignored.

In a similar fashion, it can be shown that the error in estimating frequency offset is

$$\mathrm{var}(\hat{f}_d - f_d) \geq \frac{N_o}{2|\alpha|^2\left(\zeta_t^2 - \frac{1}{E_s}\mu_t^2\right)} \tag{8}$$

where $\zeta_t^2 \triangleq \int (2\pi t)^2 |g(t)|^2 dt$ is often referred to as the mean-square duration, while $\mu_t \triangleq \int 2\pi t |g(t)|^2 dt$ is the mean time.

To translate the estimation bounds on time-delay and frequency-offset to bounds on range and radial velocity, the following relations hold:

$$\text{var}(\hat{R} - R) = \frac{c^2}{4}\text{var}(\hat{\tau} - \tau) \tag{9}$$

$$\text{var}(\hat{v} - v) = \frac{c^2}{4f_c^2}\text{var}(\hat{f}_d - f_d). \tag{10}$$

B. Angle and Angle Rate Measurement

For a scanning antenna system, the received signal response to a point target[1] is given by

$$s_r(\theta) = E(\theta - \theta_0)\alpha + w(\theta) \tag{11}$$

where $E(\theta)$ is the electric field distribution due to the antenna (assumed to be symmetric in the orthogonal ϕ domain), θ_0 is the angle of the point target, and $w(\theta)$ is a noise term. This equation is of the same form as (3) as given for the range measurement. To measure the angular rate of change of a moving target, it is beneficial to be able to measure phase changes, as the angular rate of change generally imparts very small angle changes. In order to measure phase changes due to angular motion, a spatial carrier must be applied in a fashion similar to the modulation of a temporal waveform. Such spatial carrier frequencies are applied in radio interferometric techniques [10], [11]. One method to impart a spatial carrier is to utilize a two-element interferometer where two received signals are multiplied and integrated, and then take the square root of the resulting signal. If the two signals at the elements are identical except for a time delay between the two of $\tau = (d/c)\sin\theta$, the received signal can be shown to be

$$s_r(\theta) = \sqrt{\langle s_1(t,\theta)s_2(t,\theta)\rangle} = E(\theta)e^{-j2\pi\frac{d}{2\lambda}\sin(\theta)}\alpha + w(\theta) \tag{12}$$

where $\lambda = c/f_c$. Typically, radio interferometric receivers multiply and integrate the two element signals. In this case, as will be apparent later, it is beneficial to take the square root such that the signal is proportional to the electric field distribution.

If the object is in motion with angular velocity ω rad/s, the angle of the object becomes $\theta_0 + \omega t$, and the signal response is of the form

$$s_r(\theta) = E(\theta - \theta_0 - \omega t)e^{-j2\pi\frac{d}{2\lambda}\sin(\theta-\theta_0-\omega t)}\alpha + w(\theta). \tag{13}$$

Considering angles near broadside to the interferometer, the term $\sin(\theta) \approx \theta$, and the received signal is given by

$$s_r(\theta) = E(\theta - \theta_0 - \omega t)e^{-j2\pi\frac{d}{2\lambda}(\theta-\theta_0-\omega t)}\alpha + w(\theta). \tag{14}$$

Because the object is in motion, multiple measurements must be taken over a time interval in order to measure the time rate of change of the angle. For a sample rate of f_s Hz and a spatial sampling interval $\Delta\theta$, the spatial sample rate can be defined as $f_\theta = \Delta\theta f_s$ rad/s. The angle is given by $\theta = f_\theta t$, and the received signal can be written

$$s_r(\theta) = E\left(\theta - \theta_0 - \frac{\omega}{f_\theta}\theta\right)e^{-j2\pi\frac{d}{2\lambda}\left(\theta-\theta_0-\frac{\omega}{f_\theta}\theta\right)}\alpha + w(\theta). \tag{15}$$

Equation (15) can be simplified as follows. First, in the exponential, the term $\theta_0 d/2\lambda$ is a constant, and thus $e^{j2\pi\theta_0 d/2\lambda}$ represents a constant phase term and can be subsumed into α. Second, the argument of the envelope term can be simplified by noting that the term ω/f_θ is in many cases very small and can be neglected. For example, an object at a distance of 10 m with a linear velocity of 1 m/s yields an angular velocity of 0.1 rad/s. For a relatively low receiver sample rate of 1 kHz and a spatial interval of 1°(0.017 rad) the spatial sample rate is $f_\theta = 17$ rad/s, which is significantly larger than ω, and thus the term $\theta - \theta_0 - \omega\theta/f_\theta \approx \theta - \theta_0$ since the amplitude variation due to $\omega\theta/f_\theta$ is very small. Situations where ω/f_θ is large are not considered in this paper. The received signal can therefore be simplified to

$$s_r(\theta) = E(\theta - \theta_0)e^{-j2\pi\frac{d}{2\lambda}\left(\theta-\frac{\omega}{f_\theta}\theta\right)}\alpha + w(\theta). \tag{16}$$

Defining

$$f_\omega = \frac{d\omega}{2\lambda f_\theta} \tag{17}$$

results in

$$s_r(\theta) = E(\theta - \theta_0)e^{j2\pi f_\omega\theta}e^{j2\pi\frac{d}{2\lambda}\theta}\alpha + w(\theta) \tag{18}$$

which is nearly the same form as (4), however, with the additional multiplicative term $e^{j2\pi(d/2\lambda)\theta}$. This term represents the modulation onto the spatial carrier frequency $(d/2\lambda)$. The signal form in (4) is a baseband formulation, indicating that the signal has been demodulated from the temporal carrier frequency to baseband. A similar operation can be accomplished with a scanning system, thus the baseband formulation of (18) is given by

$$s_r(\theta) = E(\theta - \theta_0)e^{j2\pi f_\omega\theta}\alpha + w(\theta) \tag{19}$$

which is the same form as (4).

In calculating the variance on the estimate of angle and angle rate measurements the signal is defined in the spatial domain as a function of the antenna. In particular, the current distribution on the aperture $J(z)$ is analogous to the time waveform $s(t)$, and the electric field distribution $E(\theta)$ to the spectral signal $S(f)$.

The electric field distribution can be found in terms of the current on the aperture, and is given in general by [11]

$$\bar{E} = -jk\eta g(r)(\hat{\theta}a_\theta + \hat{\phi}a_\phi) \tag{20}$$

where $k = 2\pi/\lambda$ is the wavenumber, $\eta = \sqrt{\mu/\epsilon}$ is the intrinsic impedance of the propagation medium (with μ and ϵ the permeability and permittivity, respectively), $g(r) = e^{-jkr}/4\pi r$ is Green's function, and a_θ and a_ϕ are given by

$$a_\theta = \cos(\theta)\cos(\phi)\tilde{J}_x + \cos(\theta)\sin(\phi)\tilde{J}_y - \sin(\theta)\tilde{J}_z \tag{21}$$

$$a_\phi = -\sin(\phi)\tilde{J}_x + \cos(\phi)\tilde{J}_y \tag{22}$$

[1]The response to multiple targets or a distributed target is in general a convolution of the target spatial distribution and the antenna pattern; this expansion of the present analysis is not considered here.

where $\tilde{J}_{x,y,z}$ are components of the Fourier transform of the current distribution on the aperture

$$\tilde{J}(k_x, k_y, k_z) = \int J(x', y', z') e^{j(k_x x' + k_y y' + k_z z')} dx' dy' dz'. \tag{23}$$

The electric field distribution is in general thus a rather complicated function of the current distribution. However, considering the current in one dimension simplifies the analysis, and the resulting electric field distribution can be shown to be

$$E(\theta) = \int_{-\infty}^{\infty} J(z) e^{j2\pi z \sin(\theta)/\lambda} dz. \tag{24}$$

The electric field distribution is thus related to the current distribution through a Fourier transform, where the current is given by

$$J(z) = \int_{-\pi}^{\pi} E(\theta) e^{-j2\pi z \sin(\theta)/\lambda} d\theta. \tag{25}$$

These integral forms can be made identical to the time-frequency integrals through a change of variables. Let $\gamma = \sin(\theta)$; then, $d\gamma = \cos(\theta) d\theta$, and

$$d\theta = \frac{d\gamma}{\cos\theta} = \frac{d\gamma}{\sqrt{1-\gamma^2}}. \tag{26}$$

For angles near broadside to the aperture, the above can be simplified since θ is small and $\sin(\theta) \ll 1$ and thus $d\theta \approx d\gamma$. The current distribution is then given by

$$J(z) = \int_{-\infty}^{\infty} E(\gamma) e^{j2\pi z_\lambda \gamma} d\gamma \tag{27}$$

where $z_\lambda = z/\lambda$.

With the above Fourier transform relationship, the angle and angle rate lower bounds can be determined using (2) as was done for the estimates of range and range rate, where the signal form is now given by

$$s_r(\gamma) = E(\gamma - \gamma_0) e^{j2\pi f_\omega \gamma} \alpha + w(\gamma). \tag{28}$$

From (2), the measurement error is therefore lower bounded as

$$\mathrm{var}(\hat{\gamma_0} - \gamma_0) \geq \frac{N_o}{2|\alpha|^2 \left(\zeta_z^2 - \frac{1}{E_s}\mu_z^2\right)} \tag{29}$$

where $E_s \triangleq \int |E(\theta)|^2 d\theta = \int |J(z)|^2 dz$. The term $\zeta_z^2 \triangleq \int (2\pi z_\lambda)^2 |J(z)|^2 dz$ is the mean-square aperture, and is the second moment of the current distribution. Likewise $\mu_z \triangleq \int 2\pi z_\lambda |J(z)|^2 dz$ is the first moment of the current distribution.

Similar to the estimate of the radial velocity through the Doppler frequency, the lower bound on the angle rate estimate is obtained using the model (28) applied in (2). From (2), the measurement error is lower bounded as

$$\mathrm{var}(\hat{f}_\omega - f_\omega) \geq \frac{N_o}{2|\alpha|^2 \left(\zeta_\gamma^2 - \frac{1}{E_s}\mu_\gamma^2\right)}. \tag{30}$$

The term $\zeta_\gamma^2 \triangleq \int (2\pi\gamma)^2 |E(\gamma)|^2 d\gamma$ is the mean-square electric field, and is the second moment of the electric field. Likewise $\mu_\gamma \triangleq \int 2\pi\gamma |E(\gamma)|^2 d\gamma$ is the first moment of the electric field distribution.

TABLE I
RADAR MEASUREMENTS AND ACCURACY PARAMETERS

Measurement	Accuracy Parameter
Range	Mean square bandwidth ζ_f
Range rate	Mean square time duration ζ_t
Angle	Mean square aperture ζ_z
Angle rate	Mean square electric field ζ_γ

C. Summary

The accuracy of the measurements of range, range rate, angle, and angle rate are dependent each on a particular set of parameters ζ and μ, each of which is of identical mathematical form, and each of which defines the effective extent of the signal in the Fourier domain opposite the parameter of interest. Because most signals are symmetric about an origin, the first moments μ are zero, and the variance depends only on the second moments ζ. Because the accuracy bounds are given by the variance, it is not unexpected that the mean terms should be present in the general case, since the variance of a random variable x is given by $\mathrm{var}(x) = E(x^2) - (E(x))^2$, where the last term is the signal mean; however, in the following, it is assumed that the means are zero. This is a reasonable assumption since in many cases the definition of the origin is arbitrary, and the mean can therefore be set to zero simply by defining the origin to be the center of the distribution.

The parameters affecting the accuracies of the four radar measurements are then given as follows. The measurement accuracy of range is dependent on the effective bandwidth of the signal

$$\zeta_f^2 = \int (2\pi f)^2 |S(f)|^2 df. \tag{31}$$

The measurement accuracy of range rate is dependent on the effective time duration of the signal

$$\zeta_t^2 = \int (2\pi t)^2 |s(t)|^2 dt. \tag{32}$$

The measurement accuracy of angle is dependent on the effective aperture distribution

$$\zeta_z^2 = \int (2\pi z_\lambda)^2 |J(z)|^2 dz \tag{33}$$

and the measurement accuracy of angle rate is dependent on the effective electric field distribution, which is given by

$$\zeta_\gamma^2 = \int (2\pi\gamma)^2 |E(\gamma)|^2 d\gamma. \tag{34}$$

The parameters effecting the four radar measurements are summarized in Table I.

III. ANALYSIS OF THE THEORETICAL ACCURACY

The variances of the four measurements are each inversely proportional to a function of the form

$$\zeta^2 = \int (2\pi\phi)^2 |S(\phi)|^2 d\phi \tag{35}$$

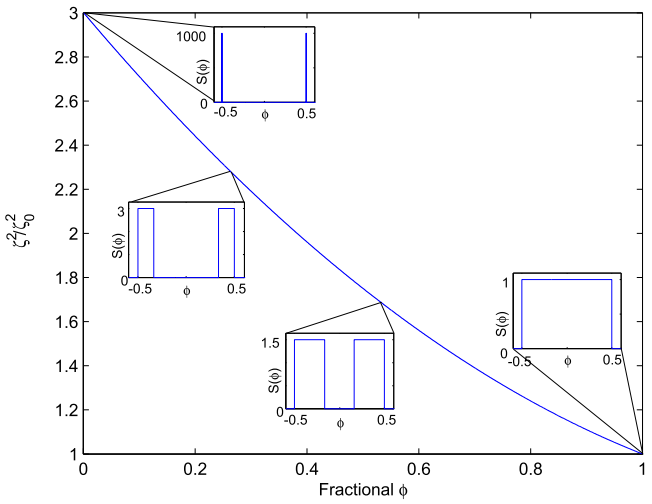

Fig. 1. Relative variation of ζ^2 as a function of the fractional extent in ϕ of two signals separated by the same total extent. The insets show the shape of the signal, where ζ_0 is the signal occupying the total extent in ϕ (far right). As the energy is concentrated toward the limits of the extent in ϕ the function ζ increases.

where ϕ represents one of $[f, t, z_\lambda, \gamma]$. In order to improve radar measurement accuracy, the variance should be minimized, and from (35), it is apparent that ζ should thus be maximized. It is instructive therefore to consider the effect of a few forms of the signal on ζ.

Fig. 1 shows the effect on ζ of altering the distribution of $S(\phi)$ where the fractional ϕ (the proportion of the signal window occupied by the signal) the varies between 0 and 1. The function ζ_0 is defined when the signal occupies the full range extent, and the ratio ζ^2/ζ_0^2 is plotted for different distributions of $S(\phi)$. The signal energy is concentrated toward the limits of the range as the abscissa approaches zero, thus when the fractional ϕ is unity, the signal occupies the full range. When the fractional ϕ is zero, the energy is concentrated into two impulses at the ends of the range, while maintaining the same total energy. As the energy is pushed toward the ends of the range, ζ^2 increases by up to a factor of three, thereby reducing the variance of the estimate. To decrease the variance on the estimate of a given parameter, the signal should in the Fourier domain concentrate the energy into two widely separated impulses. The implications of this for the four radar measurements are discussed in the following.

Comparing to Fig. 1, maximizing ζ_f is accomplished by concentrating the spectral energy of the signal into two widely separated frequency tones. Typically, radar range measurements are improved by increasing the waveform bandwidth, with the general rule-of-thumb that the measurement of range is improved with increases in the signal bandwidth. However, as Fig. 1 indicates, simply increasing the bandwidth does not optimally improve the range accuracy; for the best range accuracy two frequency tones should be used. Similarly, to improve the accuracy of the measurement of frequency, the signal should be modified to utilize two high-energy temporal pulses separated by a long length of time, rather than simply increasing the time duration (as is typically done for improved frequency measurements).

While the optimal form of the signal in its Fourier domain yields improved accuracy, additional significant benefits can be further gained by leveraging the sparsity of the optimal Fourier domain distribution to simplify the physical implementation of the system. For example, the estimation of time delay requires signal extent in the frequency domain, but it is nonoptimal to utilize uniform frequency coverage. Using a signal comprised of only two narrowband signals widely separated in frequency can greatly simplify the physical implementation of a system if the bandwidth is required to extend across a large fractional bandwidth. Implementing a signal with 10 GHz of bandwidth on a 15 GHz carrier entails significant hardware implications, including passband ripple, upconversion, and downconversion, and, importantly, the ability to sample a signal of such bandwidth. In comparison, it is much more feasible to imagine the implementation of two separate, narrowband signals located at 10 and 20 GHz; individually narrowband, the signals can be sampled effectively with low-rate digitizers, and passband nonidealities are significantly reduced. Another direct example is that of angle estimation, where one can conceive of implementing two small antennas separated by a wide baseline in comparison to implementing a single large antenna covering the full aperture. A direct example of this is given in Section IV.

What is not captured in the above analysis is the effect on resolution. With the signal energy concentrated into the sidebands, the result is a highly ambiguous measurement, and these ambiguities must be resolved in some fashion. However, for cooperative systems, such as a coherent distributed RF system, a single strong reflection or retransmission can be used, easing range diambiguation significantly.

Comparing to the accuracy for range and range rate, the above formulations of ζ_z and ζ_γ indicate that for improved angle accuracy, the current on the aperture should be confined to two strong points at the ends of the aperture, and similarly that for improved angle rate accuracy the electric field should be concentrated into two widely separated and narrow directions.

The estimate of angle using two discrete current impulses implies that two widely separated antennas can be utilized for angle estimation, and indeed such systems are employed in phase interferometers [12]. The issue again is one of disambiguation, and often in phase interferometer systems one large baseline, yielding an accurate but ambiguous angle measurement, is coupled with a narrower baseline, yielding a unambiguous but inaccurate angle measurement. This is entirely analogous to the ranging system demonstrated in [13], which made use of a continuous two-tone waveform, yielding an accurate but ambiguous range measurement, interleaved with a small-bandwidth pulse, yielding an unambiguous but inaccurate range measurement.

The estimate of a given parameter depends on the measurement of the signal in its Fourier complement domain, and thus the improvements achieved using the dual-impulse signal, where the energy is concentrated to the sidebands, in comparison to the pulse signal, where the energy is uniformly distributed, can be interpreted directly in terms of the Fourier domain representations of the signals. Often, the most practical

signal implementation is the pulse signal, represented by

$$s_1(\theta) = \Pi\left(\frac{\theta}{\Delta\theta}\right) A e^{j\theta\phi} \tag{36}$$

where

$$\Pi\left(\frac{\theta}{\Delta\theta}\right) = \begin{cases} 1, & -\frac{\Delta\theta}{2} \le \theta \le \frac{\Delta\theta}{2} \\ 0, & \text{otherwise} \end{cases} \tag{37}$$

is the unit pulse function. In the Fourier domain, the signal is a sine function

$$S_1(\phi) \propto \text{sinc}\left(\frac{\Delta\theta}{2}\phi\right) \tag{38}$$

with a width of $\Delta\phi_1 = 4\pi/\Delta\theta$. Because the primary peak in the sine function is greater than the next highest peak by 13.465 dB, there generally exists no confusion when selecting the peak corresponding to the correct location of the signal, except in very low SNR situations, and thus the measurement is unambiguous.

The optimal signal for the greatest accuracy is a dual-impulse signal with separation $\Delta\theta$, given by

$$s_2(\theta) = \left[\delta\left(\theta + \frac{\Delta\theta}{2}\right) + \delta\left(\theta - \frac{\Delta\theta}{2}\right)\right] A e^{j\theta\phi} \tag{39}$$

where $\delta(\theta)$ is the Dirac delta function. In the Fourier domain, this signal is a sinusoid

$$S_2(\phi) \propto \cos\left(\frac{\Delta\theta}{2}\phi\right) \tag{40}$$

which has a width of $\Delta\phi_2 = 2\pi/\Delta\theta$. The narrower width improves the accuracy, however, the Fourier domain signal is comprised of an infinite series of peaks, all of equal amplitude. Additional information is therefore necessary in order to disambiguate the measurement and determine the correct location of the signal. After disambiguation, the measurement accuracy is improved relative to the pulse signal, which has no ambiguities.

There exist numerous methods to disambiguate such signals. These include interleaving a pulse of width $\Delta\theta_p$ between two impulses with separation $\Delta\theta \gg \Delta\theta_p$; implementing a third impulse separated from one of the two impulses by $\Delta\theta_p \ll \Delta\theta$; or using two narrow pulses of width $\Delta\theta_p$ separated by $\Delta\theta \gg \Delta\theta_p$. In the following, examples are given of implementations of the optimal or near-optimal signal form the four radar measurements, and their relation to the optimal accuracy signal are discussed.

IV. Examples

This section summarizes examples of signal implementations used in the three traditional radar measurements as well as that used in the newer angle rate measurement. Comparisons are made to the general accuracy parameter form by computing the ratio ζ^2/ζ_0^2 and comparing to the optimal result $\zeta^2/\zeta_0^2 = 3$. It will be seen that some existing measurements approach the optimal form, and entail significant hardware implementation benefits over a uniform Fourier domain signal distribution, whereas others can approach the optimal form in unique implementations that are not typically used. The examples below are not an exhaustive review of all the measurement techniques possible, rather they are meant to help place the angle rate measurement within the context of other measurements.

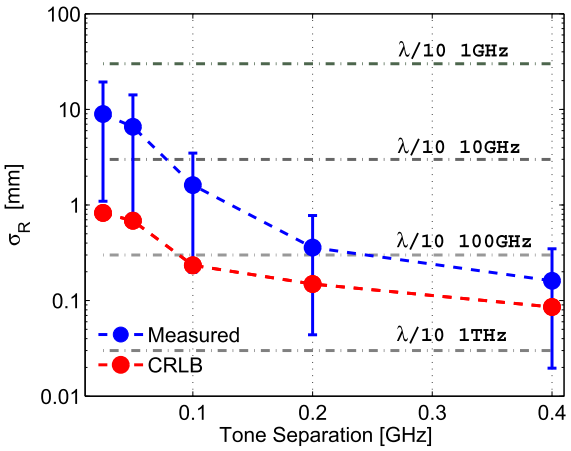

Fig. 2. X-band ranging system measured accuracy using a two-tone CW signal, approximating the optimal form for accuracy [13].

A. Range Measurement

Radar systems typically resolve range ambiguities through modulation, either in amplitude or phase, on the transmit signal, yielding a time-stamp whereby the correct range can be discerned [14]–[16]. While disambiguating the correct range of the target, typical modulation formats such as amplitude pulses or linear frequency sweeps occupy the full bandwidth of the signal, which yields a fractional $\phi = 1$ and which, as was shown above, is not optimal in terms of accuracy. Multiple-frequency continuous-wave (CW) signals can be used to disambiguate [17], however, unless the additional tones are close to the ends of the spectrum the effective bandwidth will be significantly decreased from optimal. In [13], a two tone-waveform approximating the optimal dual-impulse signal was implemented for high-accuracy ranging on microwave carrier frequencies. In that work, accuracies of below 1 mm were achieved with tone separations below 400 MHz (Fig. 2). The highly ambiguous response yielded by correlating the transmit signal with the return signal was disambiguated by periodically transmitting a low bandwidth ($\le$20 MHz) pulse and tracking the correct ambiguity lobe (Fig. 3). The ranging system was further aided by the use of a cooperative target, which retrodirected the signal back to the ranging system. In this way, one strong scattering point yielded a single correct ambiguity lobe that was uncorrupted by reflections from other scattering points. Because the system utilized a two-tone signal, in the limit that the return signal was measured for a long time duration the accuracy of the system approaches the best possible accuracy, with fractional $\phi \to 0$. The system in [13] implemented a disambiguation pulse in 1 Hz intervals, however, increasing that rate does not appreciably effect the accuracy. For example, utilizing a disambiguation pulse in 100 Hz intervals with a 9 ms two-tone waveform yields a bandwidth on each tone of 111 Hz. With a 100 MHz tone separation, the tones still occupy a negligible bandwidth, yielding a relative effective bandwidth of $\zeta_f^2/\zeta_{f0}^2 \approx 3$.

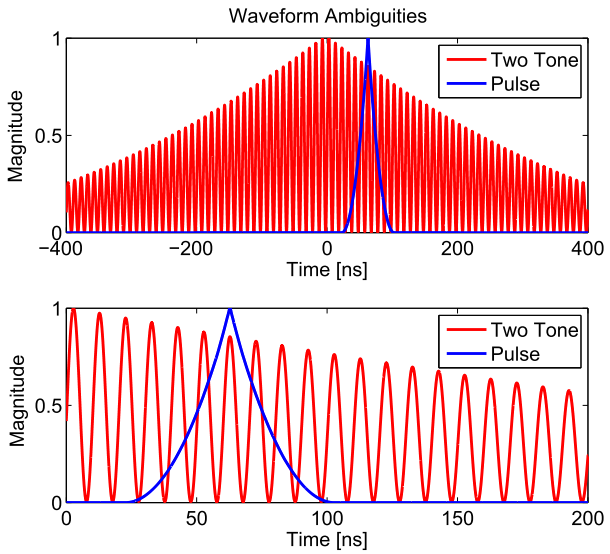

Fig. 3. Two-tone signal and pulse disambiguation in the microwave ranging system presented in [13]. The two-tone signal provides good accuracy but an ambiguous measurement, while the pulse waveform yields the opposite.

B. Range Rate Measurement

Doppler radar systems utilize either CW signals or coherent pulse trains, which are in essence temporally sampled CW signals. Whereas the CW signal represents a relative effective time duration $\zeta_t^2/\zeta_{t0}^2 = 1$, a CW signal sampled at only two points utilizes a smaller fractional time duration. Pulse trains are utilized in order to increase the peak power of the radar, increasing the detection range, while keeping the average power lower, easing concerns such as cooling and power delivery. A typical radar may use pulses that occupy only 1/20 of the time between pulses [18]. A waveform comprising seven pulses in a pulse train yields $\zeta_t^2/\zeta_{t0}^2 = 1.33$; a three-pulse waveform yields $\zeta_t^2/\zeta_{t0}^2 = 1.99$, still much lower than a two-pulse waveform with $\zeta_t^2/\zeta_{t0}^2 = 2.97$, which is not far from the optimal case $\zeta^2/\zeta_0^2 = 3$.

C. Angle Measurement

Phase interferometers utilize widely separated antennas to facilitate direction finding, or angle measurement. With two widely separated antennas with small physical apertures the signal approximates the dual-impulse signal. The antenna pattern generated by two antennas separated by a baseline D_1 consists of ambiguities that can be resolved by including a third antenna spaced closely to one of the others by $D_2 < D_1$ (Fig. 4) in a multiple baseline interferometer format [12]. Using $D_2 = D_1/10$ yields a relative effective aperture of $\zeta_z^2/\zeta_{z0}^2 = 2.6388$, whereas reducing the second baseline further to $D_2 = D_1/100$ yields $\zeta_z^2/\zeta_{z0}^2 = 2.9594$, which is close to the optimal case.

D. Angle Rate Measurement

The parameter of interest in the measurement of angle rate is the electric field distribution of the antenna system, as was derived in Section II. The electric field pattern is of interest

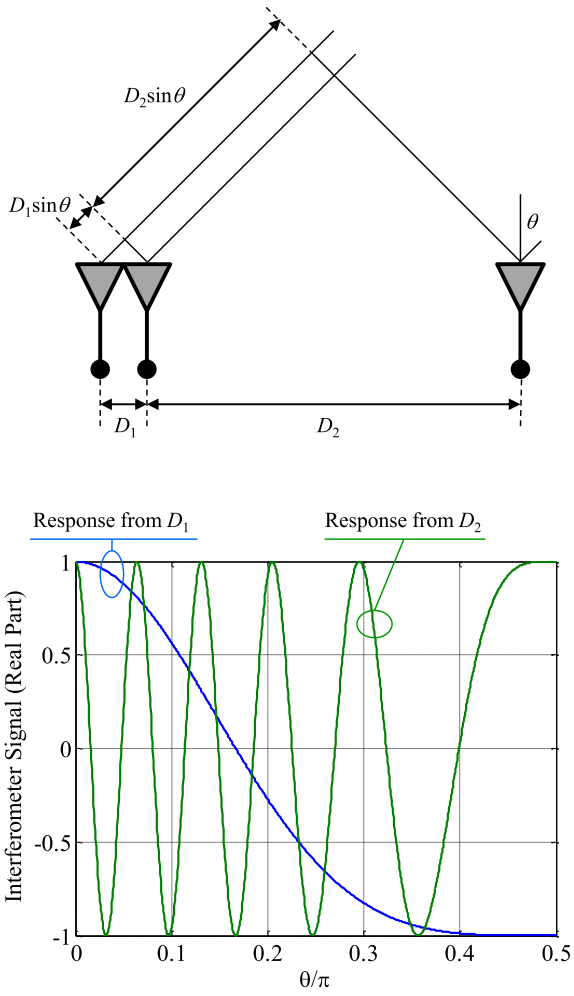

Fig. 4. Interferometer direction finding layout (top) and signal responses from the two baselines (bottom) for separations of $1/2\lambda$ and 5λ. The wide baseline provides good accuracy but an ambiguous measurement, while the narrow baseline provides the opposite. Combined, the system achieves both accuracy and disambiguation.

in general as it is one of the basic spatial parameters, along with the aperture current distribution, in an analogous fashion to the time and frequency parameters in range and range rate measurements. As derived above, the optimal shape of the electric field pattern of an antenna performing accurate angle rate measurements is a dual pencil-beam shape. There are various methods that could be employed to generate dual-beam patterns, from simple two-antenna systems to dual-feed reflector antennas.[2] One of the more direct implementations is a phased array with two outputs, each corresponding to the steering vectors of the two desired beams. Such a dual-beam phased array can be implemented with two sets of fixed beamforming weights, or generated digitally in an element-level digital array.

The electric field of a receiving phased array can be calculated by considering the transmit pattern of the array, due to

[2]Prior work by the authors has demonstrated the capability of measuring angle rate using a dual-antenna configuration [2]. It should be noted, however, that this earlier work did not use a near-optimal electric field pattern, a result of utilizing a different detection method than is considered in this paper, namely, a correlation receiver.

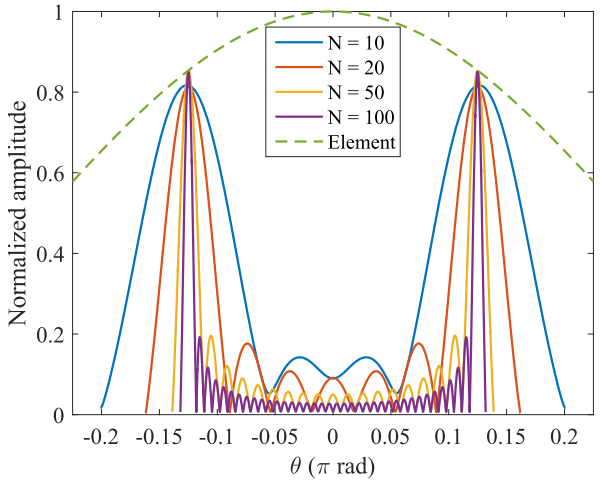

Fig. 5. Electric field pattern for a dual-beam digital array with N elements steering beams at $\pm\pi/8$ rad with varying numbers of elements. An element pattern with a beamwidth of $\pi/2$ rad was included and is shown by the dotted line. The integration limits to calculate the effective electric field pattern were taken from the first nulls outside the mainbeams, shown by the extent of the field patterns for the various numbers of elements.

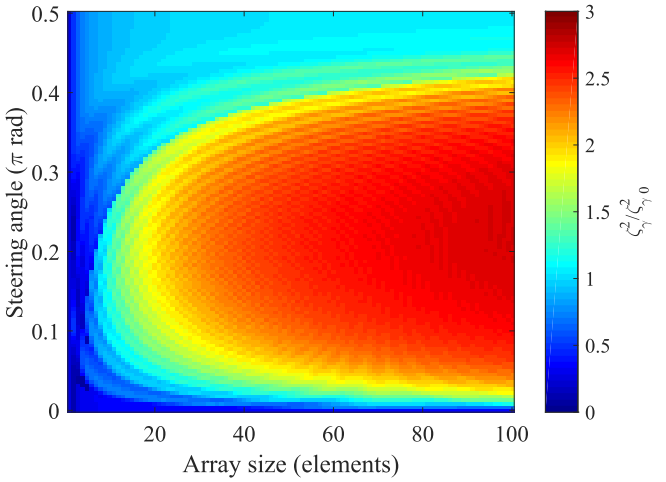

Fig. 6. Relative variation of the normalized effective electric field pattern ζ_γ^2 versus steering angle and number of elements for a digital array generating two antenna beams, calculated from the first nulls outside the two beams. The elements are spaced at intervals of $\lambda/2$, so that larger array sizes generate narrower antenna beams. An element pattern with a beamwidth of $\pi/2$ rad was included. The beams are steered at $\pm$ the steering angle. At broadside the normalized effective electric field goes to zero since the two beams converge. The sharp drop at wide steering angles results from the fact that the main beams are wide enough that nulls do not occur in the array pattern between the main beams and the extent of the field of view; for consistency the limits are taken to the ends of the field of view $\pm\pi/2$ in these cases.

reciprocity. The electric field of an N-element phased array with a single signal is given by (see [11])

$$E(\theta) = A(\theta) \sum_{n=0}^{N-1} e^{jkd\sin\theta} \tag{41}$$

where d is the interelement spacing and the harmonic dependence $e^{-j\omega t}$ is implicitly assumed. The field of two signals steered to the directions θ_1 and θ_2 is then simply

$$E(\theta) = A(\theta) \sum_{n=0}^{N-1} [e^{jkd(\sin\theta+\sin\theta_1)} + e^{jkd(\sin\theta+\sin\theta_1)}]. \tag{42}$$

Fig. 5 shows (42) with the element pattern modeled as a raised cosine function $A(\theta) = \cos^2\theta$ for array sizes of $N = 10$, 20, 50, and 100, with the beams steered to $\pm\pi/8$. As the array size increases, the beamwidth of the two beams becomes narrower, more closely approximating a dual-impulse pattern. To facilitate a comparison to the theoretically ideal signal form, ζ_γ^2 is calculated by taking the integration limits to the first nulls in the pattern beyond the two steered beams. The ideal $\zeta_{\gamma 0}^2$ is then calculated by two impulses at the location of the desired angles. The slightly lower amplitude of the $N = 10$ case is due to interference from the relatively higher sidelobes of the opposite beams, which are more pronounced when the beams are wider.

Fig. 6 shows the relative effective electric field pattern $\zeta_\gamma^2/\zeta_{\gamma 0}^2$ as a function of the array size and steering angle. The beams are steered to $\pm$ the indicated steering angle. Near broadside, $\zeta_\gamma^2/\zeta_{\gamma 0}^2 \approx 0$ since the two beams converge and have minimal or no angular separation. Toward endfire, $\pm\pi/2$ rad, the element pattern $A(\theta)$ begins to null the array pattern, also yielding low values of $\zeta_\gamma^2/\zeta_{\gamma 0}^2$. There are clear regions where $\zeta_\gamma^2/\zeta_{\gamma 0}^2 \approx 3$, notably when the beams are steered toward $\pm\pi/4$ and when the array is large. In the latter case, the beams become narrow, more closely approximating the ideal form. The sharp drop at wide steering angles results from the fact that with wide beams directed toward wide angles the array pattern does not result in a null between the mainbeam and $\pm\pi/2$. In these cases, the limits of integration for calculating ζ_γ^2 are taken to the ends of the field of view, $\pm\pi/2$.

V. Parameter Relationships and Simultaneous Measurements

The four radar measurements can clearly be grouped into two sets of measurements—one including range and range rate, the other angle and angle rate—that can be performed simultaneously. The simultaneous measurement of these depends on the relationship between the parameters relevant to each measurement. The simultaneous measurement of range and range rate depends on both the bandwidth and time duration of the temporal signal, respectively. Likewise, the simultaneous measurement of angle and angle rate depends on the spatial signal extent (aperture size) and spatial frequency coverage (electric field pattern). Being fundamentally related, the impact on measurement error of the effective time-bandwidth and aperture-pattern products can be assessed.

With the individual measurement accuracies of range and range rate given by (7) and (8), the error of the simultaneous measurement of range and range rate is

$$\sigma_{t,f} = \sqrt{\mathrm{var}(\hat{\tau}-\tau)\mathrm{var}(\hat{f}_d - f_d)} = \frac{N_0}{2E\zeta_f\zeta_t}. \tag{43}$$

The effective time-bandwidth product is given by

$$\zeta_f\zeta_t = \sqrt{\frac{\int (2\pi t)^2|s(t)|^2dt \int (2\pi f)^2|S(f)|^2df}{\int |s(t)|^2dt \int |S(f)|^2df}}. \tag{44}$$

It can be shown [11], [19] that for signals of finite time duration the above reduces to

$$\zeta_f\zeta_t \geq \pi \tag{45}$$

and thus the accuracy of the simultaneous measurement is

$$\sigma_{t,f} \leq \frac{N_0}{2\pi E}. \tag{46}$$

The same result is found for the simultaneous measurement of angle and angle rate

$$\sigma_{\gamma,f_\omega} = \sqrt{\mathrm{var}(\hat{\gamma} - \gamma)\mathrm{var}(\hat{f_\omega} - f_\omega)} = \frac{N_0}{2E\zeta_z\zeta_\gamma} \tag{47}$$

and the effective aperture-pattern product is then

$$\zeta_z\zeta_\gamma = \sqrt{\frac{\int (2\pi z/\lambda)^2 |J(z)|^2\, dz \int (2\pi\gamma/\lambda)^2 |E(\gamma)|^2\, d\gamma}{\int |J(z)|^2\, dz \int |E(\gamma)|^2\, d\gamma}} \tag{48}$$

and the same procedure applies as to the effective time-bandwidth product, yielding

$$\zeta_z\zeta_\gamma \geq \pi \tag{49}$$

and thus

$$\sigma_{\gamma,f_\omega} \leq \frac{N_0}{2\pi E}. \tag{50}$$

While the bandwidth of a temporal signal is inversely related to timing characteristics of the signal, such as the rise time of a pulse, and therefore places a lower limit on the time-bandwidth product, the bandwidth can be increased beyond this through other means. For example, a linear frequency modulation sweeps the center frequency of the temporal signal over a certain bandwidth, which can exceed that of the inverse of the rise time. The time-bandwidth product can thus be increased arbitrarily, thereby improving the accuracy of the simultaneous measurement of range and range rate, ultimately with limitations imposed by the capabilities of the system hardware.

In a similar manner the width of the electric field pattern is inversely related to the spatial extent of the aperture in a spatial signal, imposing a lower limit on the aperture-pattern product. However this can also be increased through means such as sweeping the frequency in the same manner as in a temporal signal. For example, the spatial pattern of a two-antenna system is defined in part by the separation of the two antennas measured in wavelengths, thus by sweeping the wavelength the pattern spans a range of spatial frequencies. The aperture-pattern product can thus be increased arbitrarily, improving the accuracy of the simultaneous measurement of angle and angle rate.

VI. Conclusion

Whereas direct angle rate measurements have not traditionally been implemented in radar systems, the current drive toward digital arrays and coherent distributed arrays provides pathways toward a practical use of the measurement. The optimal form for accurate angle rate measurements has been shown here to be a dual-beam electric field pattern, which can be implemented in a digital array or dual-antenna system. Furthermore, coherent distributed arrays provide a means for achieving simultaneously accurate angle measurements due to potentially long baselines. Future radar systems may see significant improvements in target tracking by combining direct angle rate measurements with the standard radar measurements.

In general, the optimal signal forms (whether for range, range rate, angle, or angle rate measurements) should be considered where accuracy is needed. Improved accuracy is nonetheless not free, and the resulting ambiguities of more accurate measurements must be resolved. This resolution can be simple, as in the case of cooperative systems that can provide additional information for disambiguation, but is also not necessarily difficult in noncooperative systems, as the targets may be approximated by point targets (as in the case of angle measurements), easing ambiguity problems. Future work lies in experimental implementations of joint measurements of the four radar parameters, simultaneously achieving high accuracy for multiple measurements.

References

[1] J. A. Nanzer, "Millimeter-wave interferometric angular velocity detection," *IEEE Trans. Microw. Theory Techn.*, vol. 58, no. 12, pp. 4128–4136, Dec. 2010.

[2] J. Nanzer and K. Zilevu, "Dual interferometric-Doppler measurements of the radial and angular velocity of humans," *IEEE Trans. Antennas Propag.*, vol. 62, no. 3, pp. 1513–1517, Mar. 2014.

[3] J. A. Nanzer, "On the resolution of the interferometric measurement of the angular velocity of moving objects," *IEEE Trans. Antennas Propag.*, vol. 60, no. 11, pp. 5356–5363, Nov. 2012.

[4] H. Ochiai, P. Mitran, H. V. Poor, and V. Tarokh, "Collaborative beamforming for distributed wireless ad hoc sensor networks," *IEEE Trans. Signal Process.*, vol. 53, no. 11, pp. 4110–4124, Nov. 2005.

[5] R. Mudumbai, G. Barriac, and U. Madhow, "On the feasibility of distributed beamforming in wireless networks," *IEEE Trans. Wireless Commun.*, vol. 6, no. 5, pp. 1754–1763, May 2007.

[6] D. R. Brown, III, and H. V. Poor, "Time-slotted round-trip carrier synchronization for distributed beamforming," *IEEE Trans. Signal Process.*, vol. 56, no. 11, pp. 5630–5643, Nov. 2008.

[7] H. Chen, A. B. Gershman, and S. Shahbazpanahi, "Filter-and-forward distributed beamforming in relay networks with frequency selective fading," *IEEE Trans. Signal Process.*, vol. 58, no. 3, pp. 1251–1262, Mar. 2010.

[8] J. A. Nanzer, R. L. Schmid, T. M. Comberiate, and J. E. Hodkin, "Open-loop coherent distributed arrays," *IEEE Trans. Microw. Theory Techn.*, to be published, doi: 10.1109/TMTT.2016.2637899.

[9] H. L. Van Trees, *Detection, Estimation, and Modulation Theory*, vol. 3. Hoboken, NJ, USA: Wiley, 2001.

[10] A. R. Thompson, J. M. Moran, and G. W. Swenson, Jr., *Interferometry and Synthesis in Radio Astronomy*. Hoboken, NJ, USA: Wiley, 2001.

[11] J. A. Nanzer, *Microwave and Millimeter-Wave Remote Sensing for Security Applications*. Norwood, MA, USA: Artech House, 2012.

[12] S. E. Lipsky, *Microwave Passive Direction Finding*. West Perth, WA, Australia: SciTech, 2004.

[13] J. E. Hodkin *et al.*, "Microwave and millimeter-wave ranging for coherent distributed RF systems," in *Proc. IEEE Aerosp. Conf.*, Mar. 2015, pp. 1–7.

[14] A. Stelzer, C. G. Diskus, K. Lubke, and H. W. Thim, "A microwave position sensor with submillimeter accuracy," *IEEE Trans. Microw. Theory Techn.*, vol. 47, no. 12, pp. 2621–2624, Dec. 1999.

[15] Z. M. Tsai *et al.*, "A high-range-accuracy and high-sensitivity harmonic radar using pulse pseudorandom code for bee searching," *IEEE Trans. Microw. Theory Techn.*, vol. 61, no. 1, pp. 666–675, Jan. 2013.

[16] T. Jaeschke, C. Bredendiek, S. Küppers, and N. Pohl, "High-precision D-band FMCW-radar sensor based on a wideband SiGe-transceiver MMIC," *IEEE Trans. Microw. Theory Techn.*, vol. 62, no. 12, pp. 3582–3597, Dec. 2014.

[17] A. Schicht, K. Huber, A. Ziroff, M. Willsch, and L.-P. Schmidt, "Absolute phase-based distance measurement for industrial monitoring systems," *IEEE Sensors J.*, vol. 9, no. 9, pp. 1007–1013, Sep. 2009.

[18] M. I. Skolnik, *Introduction to Radar Systems*. New York, NY, USA: McGraw-Hill, 2002.

[19] M. I. Skolnik, *Introduction to Radar Systems*. New York, NY, USA: McGraw-Hill, 1962.

Jeffrey A. Nanzer (S'02–M'08–SM'14) received the B.S. degree in electrical and computer engineering from Michigan State University, East Lansing, MI, USA, in 2003, and the M.S. and Ph.D. degrees in electrical engineering from The University of Texas at Austin, Austin, TX, USA, in 2005 and 2008, respectively.

From 2008 to 2009, he was a Post-Doctoral Fellow with the Applied Research Laboratories, The University of Texas at Austin, where he designed electrically small HF antennas and communications systems. From 2009 to 2016, he was with The Johns Hopkins University Applied Physics Laboratory, Laurel, MD, USA, where he created and led the Advanced Microwave and Millimeter-Wave Technology Section. In 2016, he joined the Department of Electrical and Computer Engineering, Michigan State University, where he is currently the Dennis P. Nyquist Assistant Professor. He has authored more than 60 refereed journal and conference papers. He has authored the book *Microwave and Millimeter-Wave Remote Sensing for Security Applications* (Artech House, 2012), and has co-authored the chapter "Photonics-Enabled Millimeter-Wave Wireless Systems" in the book *Wireless Transceiver Circuits* (Taylor Francis, 2015). His current research interests include coherent distributed arrays, microwave and millimeter-wave remote sensing, antennas and arrays, millimeter-wave photonics, radiometry, and electromagnetics.

Dr. Nanzer is a member of the IEEE Antennas and Propagation Standards Committee, the USNC/URSI Commission B, the Executive Committee for the IEEE International Conference on Ultra-Wideband, the Technical Program Review Committees for the IEEE International Microwave Symposium, and the IEEE International Conference on Microwaves for Intelligent Mobility. He was a Founding Member and the first Treasurer of the IEEE AP-S/MTT Central Texas Chapter. From 2013 to 2015, he served as the Vice-Chair of the IEEE Antenna Standards Committee. He is the Chair of the IEEE Microwave Theory and Techniques Society Microwave Systems Technical Committee (MTT-16). He was a recipient of the 2012 JHU/APL Outstanding Professional Book Award.

Matthew D. Sharp (S'06–M'11) received the B.S. degree in electrical engineering from the George Washington University, Washington, DC, USA, in 2003, the M.S. degree in electrical engineering from Bucknell University, Lewisburg, PA, USA, in 2005, and the Ph.D. degree in electrical engineering from Cornell University, Ithaca, NY, USA, in 2011.

His current research interests include distributed sensing systems, digital arrays, electronic warfare, and signal processing for radars and communications.